Universität des Saarlandes

Fachrichtung 6.1 – Mathematik

Conservative shock filtering of numerical solutions of the 1-D Euler equations

Michael Breuß

Conservative shock filtering of numerical solutions of the 1-D Euler equations

Michael Breuß

Faculty of Mathematics and Computer Science
Saarland University
Building E 1 1
66041 Saarbrücken
Germany
breuss@mia.uni-saarland.de

Abstract

We consider a recently developed conservative shock filter model in order to postprocess numerical solutions of the 1-D Euler equations of gas dynamics. The shock filtering process involves the definition of an indicator selecting the data regime where the filter is applied. Illustrated by several classical numerical test problems, we show that the use of simple indicators based on physical principles results in very accurate approximations of shocks and contact discontinuities.

1   Introduction

This paper is concerned with postprocessing numerical approximations of the *onedimensional Euler equations of gas dynamics*

$$\underline{u}_t(x,t) + \underline{f}\left(\underline{u}(x,t)\right)_x = \underline{0}, \quad x \in \mathbf{R},\, t > 0, \tag{1}$$

where $\underline{u} = [\rho, \rho v, \rho E]$ is the vector of *conserved quantities* and $\underline{f}\left(\underline{u}\right) = [\rho v, \rho v^2 + p, \rho v H]$ is the *flux function*. Thereby, the symbols ρ, ρv, ρE, p and H denote density, momentum, energy density, pressure and enthalpy, respectively, and $H := E + (p/\rho)$. The described system is supplemented by an *equation of state* defining the properties of the gas whose flow is modeled. Since (1) describes an evolution in time, one needs to define an initial condition $\underline{u}_0(x) \equiv \underline{u}(x, 0)$, and, when appropriate, suitable boundary conditions [9, 10].

Solutions of the Euler equations feature *discontinuities*, i.e., *shocks* and *contact discontinuities*. Numerical approximations usually incorporate a diffusive mechanism in order to capture shocks at the correct location, resulting, in general, in a blurring effect at strong data gradients. While a shock involves a compression naturally stabilising numerically obtained shock profiles, the approximation of a contact discontinuity usually suffers from relatively strong blurring artefacts. Many recipes were developed during the last decades to fix the adressed problems, see e.g. [7, 13, 16] and the references therein for an overview.

We now turn to the method we employ for the accurate reconstruction of discontinuities, i.e., we use a *shock filter* to remove blurring artefacts at discontinuities by a postprocessing procedure at the end of a simulation. In

contrast to the classical shock filter proposed by Osher and Rudin [15], given by

$$q_\tau(x, \tau) = -|q_x(x, \tau)| \, \mathsf{signum}\left(q_{xx}(x, \tau)\right), \tag{2}$$

the new filter we consider here is in *divergence form*. This is important in the context of the approximation of conservation laws as it is a crucial property for capturing discontinuities at correct positions. For a scalar quantity of interest $q \equiv q(x, \tau)$, $x \in \mathbf{R}$, $\tau > 0$, with a given function $q_0(x) \equiv q(x, 0)$, the onedimensional PDE identical with the shock filter model used within this paper reads

$$q_\tau(x, \tau) = G\left(\mathsf{signum}\left(q_x(x, \tau)\right) q_x(x, \tau)\right)_x. \tag{3}$$

Thereby, G is defined as

$$G(a) = \begin{cases} 0 & : & a \le 0 \\ 1 & : & a > 0 \end{cases}, \tag{4}$$

and $\mathsf{signum}(\cdot)$ denotes as usual the function given by

$$\mathsf{signum}(a) = \begin{cases} -1 & : & a < 0 \\ 0 & : & a = 0 \\ 1 & : & a > 0 \end{cases}. \tag{5}$$

Note that $G(\cdot)$ is with the exception of its definition at $G(0)$ identical with the Heaviside-function; however, we use the letter G here in order not to mess with the usual notation of enthalpy. Recently, see [4], the modeling of the PDE (3) was given as well as its rigorous validation, i.e., solutions of the initial value problem given by (3) together with $q(x, 0) = q_0(x)$ are to be understood in a distributional sense. Two numerical results concerned with scalar conservation laws were presented in [4] in order to show that a reasonable numerical realisation of (3) is possible, however, the aim of [4] was to give a solid theoretical foundation for further work. In this paper, our aim is to apply by (3) a recently developed, mathematically rigorously justified sharpening process in the context of a relevant system of equations. The main reference concerned with related topics contains algorithms derived on a heuristic basis on the discrete level [5], however, let us note that the recipes given there are primarily useful for reducing spurious oscillations and not for deblurring. Other significant attempts relying on the use of strategies from image processing are focused on the use of diffusion filters treating oscillations, see e.g. [8] and the references therein.

Considering alternative approaches to (3) for conservative shock filtering, a possible candidate is stabilised inverse diffusion. However, processes relying on stabilised inverse diffusion introduce the so-called staircasing phenomenon

[2, 3, 11]: depending on given data, piecewise constant structures reminiscent of a staircase come out as typical filtering results which can spoil a solution completely. It is a conceptual advantage of the process described via (3) that this cannot occur in corresponding solutions.

Let us now briefly comment on the computational ingredients used in this paper. Concerning the application of shock filtering within a numerical method, we prefer at the moment this paper is written a final postprocessing over a predictor-corrector-type formulation, as the need for an indicator selecting the filtering region makes the latter choice inefficient when used every time step. Thinking of a sharpening of discontinuities, a principle idea is to use a computationally inexpensive and robust method approximating the Euler equations, and to filter the numerical solution at the end, gaining accuracy. As long as the underlying numerical method introduces some amount of numerical viscosity at discontinuous solution features, this is a reasonable option. We show this by applying the same postprocessing routine for improving results generated by a monotone scheme and a second-order high-resolution central TVD method, respectively. Especially, the results show that the application of the described postprocessing procedure at a numerical solution computed using a second-order high-resolution TVD scheme can be a reasonable alternative to higher-order methods.

The content of this paper is as follows. In the second section we describe a suitable discretisation of (3). The third paragraph is devoted to a detailed description of the indicator, using a typical numerical solution of the shock tube problem in order to illuminate basic filter properties. We discuss further test cases in the numerical tests section. The paper is finished by conclusive remarks and acknowledgements.

2 Discretisation of the filter model

In this section, we develop a method suitable for discretising (3). We would like to stress that there is a certain freedom in designing an algorithm as the one we describe in the following; the motivation for our choice was coding simplicity in 1-D.

Let $\left\{Q_j^n\right\}$, $j \in \mathcal{I}$, where $\mathcal{I} \subset Z$ is an index set, be a set of scalar-valued data with

$$Q_j^n \approx q\left(j\Delta x,\, n\Delta t\right), \tag{6}$$

where Δt and Δx are uniform parameters defining an equidistant mesh. In accordance with (6), $\left\{Q_j^0\right\}$, $j \in \mathcal{I}$, defines suitable initial data for the filtering process, obtained by a numerical approximation of conservation laws.
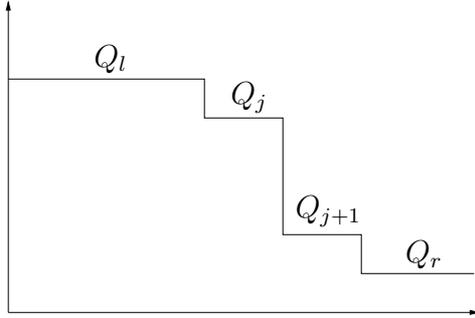
Figure 1: The figure shows a sketch of a typical data situation encountered when approximating a discontinuity.

For simplicity of the presentation, we suppose that $q_x(x, \tau) \leq 0$ holds within the region of our interest. The case $q_x(x, \tau) \geq 0$ can be dealt with analogously. At data extrema with $q_x(x-, \tau) \cdot q_x(x+, \tau) < 0$ no filtering takes place. Having in mind this simplification, the PDE (3) reduces to

$$q_\tau(x, \tau) = G\left(-q_x(x, \tau)\right)_x. \tag{7}$$

Let us now consider the situation shown in Figure 1. The result of our filtering process, applied at data as sketched there, is to move the amount $Q_{j+1} - Q_r$ onto Q_j, ideally filling up the difference $Q_l - Q_j$. Then a discontinuity represented by the data in Figure 1 is represented as accurate as the given mesh enables. Consequently, the presence of an inflow due to (7) from cell $j + 1$ into cell j is detected by $Q_{j+2} - Q_{j+1} < 0$, while no outflow from cell j into cell $j - 1$ is present since $Q_{j-1} - Q_{j-2} = 0$; if $Q_{j-1} - Q_{j-2} < 0$ would hold, the amount $Q_{j+1} - Q_{j+2}$ must be added to Q_{j-1}, compare (7). Thus, a valid discretisation of (7) for the case depicted in Figure 1 is given by

$$Q_j^{n+1} = Q_j^n + \frac{\Delta\tau}{\Delta x} \left[G\left(Q_{j+1}^n - Q_{j+2}^n\right) - G\left(Q_{j-2}^n - Q_{j-1}^n\right) \right]. \tag{8}$$

We omitted divisions by Δx within the arguments of G since these do not change the resulting function values. The degree of freedom introduced by $\Delta\tau$ we use here for *stabilisation.*
Within the discussion of the case depicted in Figure 1, a suitable definition for $\Delta\tau$ is

$$\Delta\tau = \Delta x \min\left(Q_{j-1}^n - Q_j^n, Q_{j+1}^n - Q_{j+2}^n\right) \tag{9}$$

since this choice obviously prevents oscillations. However, note that (9) is a *local* definition, valid at the index j. In general, the region where the *discrete*

4

filter given by (8) is to be applied needs to be detected by an *indicator*, see the next paragraph for a concrete example.

Let us for the moment assume that the indicator yields an interval defined by indices j_{left} and j_{right}; in Figure 1, we would have $\{j_{left}, j_{right}\} = \{j, j+1\}$. Within our code, we have defined a *marker variable* we may call here M, setting $M = 1$ if the indicator is met and $M = 0$ otherwise. Considering a grid featuring indices $\{0, \ldots, N\}$, we find j_{left} and j_{right} as follows, described in pseudocode:

$$
\text{for } i = 1 \text{ to } N - 1:
\begin{cases}
j_{left} := i & \text{if } M_{i-1} = 0 \land M_i = 1 \land M_{i+1} = 1 \\
j_{right} := i & \text{if } M_{i-1} = 1 \land M_i = 1 \land M_{i+1} = 0
\end{cases}, \tag{10}
$$

where $\land$ is the logical **and** operation, and where one can define values of M at the boundaries $\{0, N\}$ corresponding to the underlying problem. Then, the correct computation of $\Delta\tau$, analogously to (9), is given by

$$
\Delta\tau = \Delta x \min \left(Q^n_{j_{left}-1} - Q^n_{j_{left}}, Q^n_{j_{right}} - Q^n_{j_{right}+1} \right). \tag{11}
$$

A close inspection of the filter step (8) shows, that at *inner points* of a filtering region, i.e., excluding j_{left}, j_{right}, it holds

$$
G \left(Q^n_{j+1} - Q^n_{j+2} \right) = 1 \quad \text{and} \quad G \left(Q^n_{j-2} - Q^n_{j-1} \right) = 1, \tag{12}
$$

and thus the fluxes drop out except for the changes at j_{left} and j_{right}. Consequently, a filter step consists of

1. Compute j_{left} and j_{right}.

2. Compute (11).

3. Compute
$$
\begin{cases}
Q^{n+1}_{j_{left}} &= Q^n_{j_{left}} + \dfrac{\Delta\tau}{\Delta x} \\[2mm]
Q^{n+1}_{j_{right}} &= Q^n_{j_{right}} - \dfrac{\Delta\tau}{\Delta x}
\end{cases}. \tag{13}
$$

These steps need to be repeated until the indicator shows that the filtering process has come to an end. As shown by Figure 1, already a region incorporating a profile smeared over two grid points can be used for the application of the process, and thus the process is repeated until, in the above example,

$$
\eta := \sum_{i=0}^{N} M_i = 1. \tag{14}
$$

5

Two open issues are: η needs to be compared with a controlling reference value in order to determine if the filtering process is to be stopped, and we also have to take into account multiple filtering regions. In the remaining part of this section, we adress exactly these points.

The computation of a reference value for η, which we call here *counter* since it counts the number of filtering regions, is very easy: after initialising *counter* $= 0$, we can set, e.g.,

$$\text{for } i = 1 \text{ to } N \quad : \quad counter := counter + 1.0$$
$$\text{if } M_{i-1} = 0 \wedge M_i = 1, \tag{15}$$

again choosing suitable values M_0, M_N. The procedure (15) effectively takes into account a filtering region if its beginning is detected: if *counter* $= \eta$, the filtering process ends.

Thus, combining (14) and (15) one can treat multiple filtering regions. It remains to fit the computation of $\Delta\tau$ from (11) to this purpose. Within the code generating the results presented in this paper we use a very simple proceeding: we define a global filtering time step size $\Delta\tau^g$, and compare $\Delta\tau^g$ with $\Delta\tau$ every time we compute $\Delta\tau$ by means of (11). Thus, after initialising

$$\Delta\tau^g := \langle \text{large positive number compared with data differences} \rangle, \tag{16}$$

we compute, in pseudocode:

$$\text{for } i = 1 \text{ to } N - 1 :$$
$$\begin{cases} \Delta\tau^g := \min\left(\Delta\tau^g, Q_{i-1}^n - Q_i^n\right) \\ \quad \text{if } \{M_{i-1}, M_i, M_{i+1}\} = \{0, 1, 1\}, \\ \Delta\tau^g := \min\left(\Delta\tau^g, Q_i^n - Q_{i+1}^n\right) \\ \quad \text{if } \{M_{i-1}, M_i, M_{i+1}\} = \{1, 1, 0\}, \end{cases} \tag{17}$$

again with appropriate M_0, M_N. Let us note, that there is no danger in setting a very large initial number $\Delta\tau^g$ because of our indicator-type strategy from (10): either, there is a filtering region defined by at least two adjacent points with $M = 1$, then we compute at least one value $\Delta\tau$, see (11), or there is no filtering region, then *counter* $= \eta$ holds and no filtering takes place.

Let us emphasize that the discussed discretisation refers to a scalar quantity described by $\{Q_j^0\}$. In a setting concerned with systems of equations as within this paper, we apply the described filtering successively at the quantities of interest. This is necessary anyway if we do not want to treat algorithmically synchronisation problems arising by the coupling of variables. We go into more details within the next paragraph.

6

3   The indicator

In order to illustrate the construction of our indicator as well as the filtering procedure described within the preceding paragraph, we now consider the so-called *shock tube problem of Sod* which is a specific Riemann problem.

A Riemann problem is an initial value problem defined by constant states left and right of a chosen spatial point $\hat{x}$, for instance $\hat{x} = 0$. The physical equivalent of the Sod shock tube problem is given by two gas chambers separated by a membrane at $\hat{x}$, featuring on both sides of the membrane zero velocities but different densities and pressures. At $t = 0$, the membrane is removed. The shock tube problem consists of determining the solution for $t > 0$, compare [13, 16].

The initial conditions we use here are

$$[\rho_L,\, p_L,\, v_L]^T = [1,\, 1,\, 0]^T \text{ and } [\rho_R,\, p_R,\, v_R]^T = [0.125,\, 0.1,\, 0]^T, \qquad (18)$$

where the indices L and R denote the left and right initial states of the Riemann-problem, respectively.

As indicated, the 1-D Euler equations have to be supplemented by an equation of state. We use the equation of state for a *gamma-law gas*

$$\rho E = \frac{p}{\gamma - 1} + \frac{1}{2}\rho v^2, \qquad (19)$$

with $\gamma = 1.4$ which is the common choice for air [13].

The content of this paragraph is as follows. First, we briefly comment on the initial data we use for demonstrating our indicator. Then, we describe the indicators used for selectively filtering shocks and contact discontinuities, respectively. Finally, we address the coupling of variables within the Euler equations and its influence on the numerical filtering procedure.

3.1   A simple approximation of the shock tube problem

For demonstration purposes we use the *modified Lax-Friedrichs (mLF) scheme* which reads, for a scalar hyperbolic conservation law $u_t + f(u)_x = 0$,

$$U_j^{n+1} = U_j^n + \frac{1}{4}\left(U_{j-1}^n - 2U_j^n + U_{j+1}^n\right) - \frac{\Delta t}{2\Delta x}\left(f\left(U_{j+1}^n\right) - f\left(U_{j-1}^n\right)\right). \quad (20)$$

The scheme (20) introduces abundant *numerical diffusion* into a numerical solution, however, it is also one of the few schemes from which it is known that it approximates the unique physically relevant *entropy solution* [7].
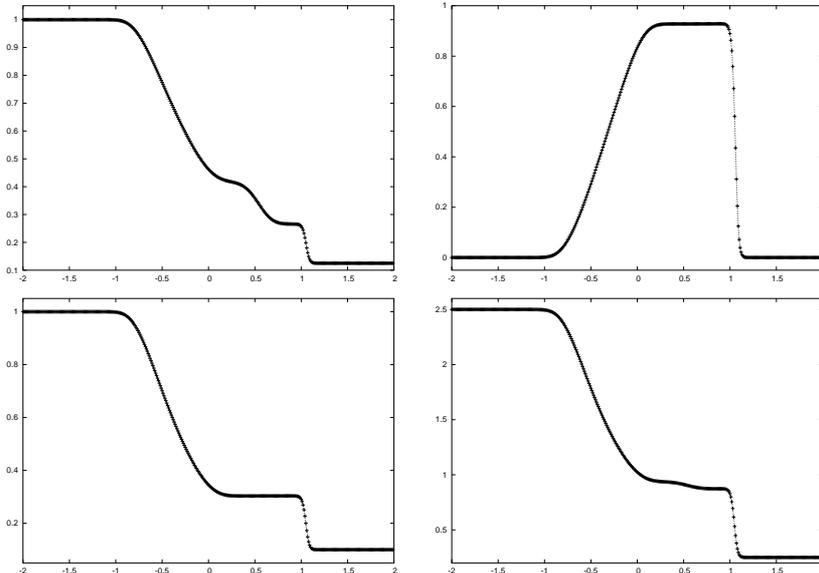
Figure 2: Diffusive artefacts within a first-order numerical approximation of the shock tube problem. **Left column:** density (top) and pressure (bottom). **Right column:** velocity (top) and total energy (bottom).

Figure 2 displays a typical numerical solution of the shock tube problem, here obtained by using (20) on a uniform mesh with a time step size determined by the CFL condition [13] so that the scheme is stable. We give the numerical solution in terms of the primitive variables ρ, v, p and E since the corresponding figures are most instructive. The solution consists of three easily distinguished features, namely a right moving shock followed by a contact discontinuity and a rarefaction wave.

We observe the effect of numerical diffusion: the profile of the right moving shock, defined especially by a jump in both density ρ and pressure p [9], as well as the profile of the contact discontinuity, defined especially by a jump in density ρ while at the same point pressure p and velocity v are continuous [9], are very smeared. Note in this context, that a blurring of the contact discontinuity is usual in numerical approximations of this problem, even when using high-order schemes. The transition from the left state $[\rho_L,\, p_L,\, v_L]^T$ to the beginning of the rarefaction wave also suffers from numerical diffusion; this artefact will not be removed by shock filtering which is, as indicated, concerned only with discontinuous solution features. It must be dealt with by another means of reducing numerical viscosity, e.g., by use of a high-resolution method as, for instance, by the second-order high-resolution *Nessyahu-Tadmor (NT)* scheme we consider within the section on numerical
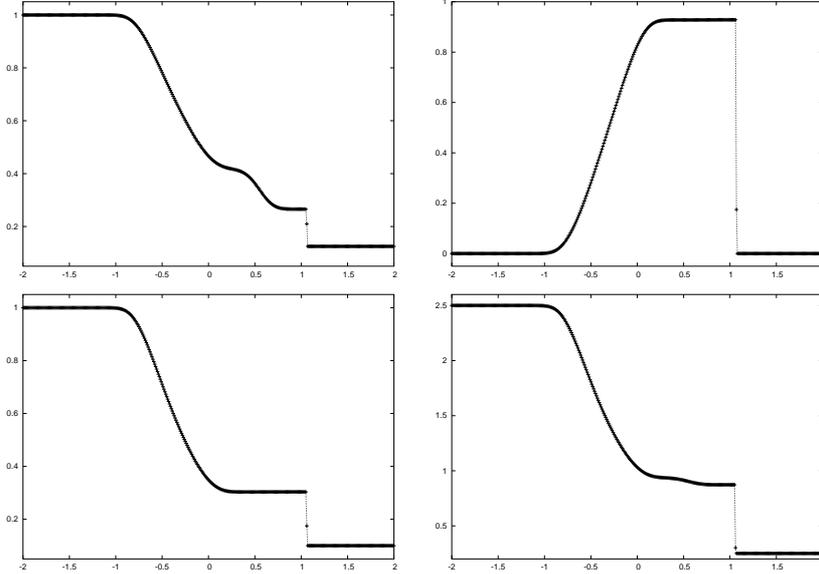
Figure 3: Selective filtering of the shock. **Left column:** density (top) and pressure (bottom). **Right column:** velocity (top) and total energy (bottom).

tests.

In the following, we use the numerical solution displayed in Figure 2 as initial data $\{Q_j^0\}$ for illustrating details of the filtering process.

3.2 The shock indicator

As an indicator for the smeared shock profile that we need in order to apply our shock filter, we use the following properties of the corresponding data, determined at any 3-tupel of data, with indices l, m and r:

$$\text{jump in pressure:} \qquad p_l > p_m > p_r \quad or \quad p_l < p_m < p_r, \qquad (21)$$

$$\text{entropy condition:} \qquad v_l > v_m > v_r. \qquad (22)$$

Let us stress, that the stated conditions are directly transfered from the physical characteristics of a shock [9]:

- Condition (21) selects data featuring a jump in pressure, which distinguishes a shock wave, for instance, from a contact discontinuity. However, as it is obvious by Figure 2, pressure also varies monotonically within a rarefaction wave.

9

- Condition (22) ensures directly the validity of the *geometrical entropy condition* due to Lax, see e.g. [12, 13]. It excludes rarefaction waves, complementing (19).

- Both conditions together ensure the numerical robustness of the indicator.

In Figure 3 we observe the effects of the shock filtering process using the indicator (21)-(22) in order to determine $\{M_i\}_{i=0,\,\ldots,\,N}$, see (10)-(17). Evidently, all shock features are approximated as sharp as possible by the given mesh.

3.3   The contact discontinuity indicator

As an indicator for filtering the contact discontinuity, the usual numerical blurring of such waves immediately suggests to use the

$$\text{spreading condition:} \qquad v_l \leq v_m \leq v_r. \tag{23}$$

Usually, the characteristics in the vicinity of a contact wave run nearly parallel; a numerical smearing of a discontinuity carried along with the underlying approximately linear flow indicates a slight spreading of numerical characteristics, i.e., (23).

However, a problem immediately appears, compare Figure 2: condition (23) also holds within rarefaction waves.

In order to distinguish a rarefaction wave from a numerically smeared contact discontinuity, we employ *in the situation $\rho_x < 0$* the so-called *local Mach number* $\mathcal{M}$ determined by

$$\mathcal{M} = \frac{|v|}{a}, \quad a = \sqrt{\gamma \frac{p}{\rho}}, \tag{24}$$

see [16]. In (24), a is the local speed of sound. The reason for the use of (24) is given by the ingredients and the physical properties of contact and rarefaction waves:

- Across a contact discontinuity, the pressure p and the velocity v can be assumed to be numerically nearly constant while there is a discontinuity in the density ρ. Thus, in such a case, the variation in a numerically determined local Mach number is dominated by the variation in ρ: if $\rho_x < 0$, also $\mathcal{M}_x < 0$.

- Within a rarefaction wave, p and ρ are linked via a constant speed of sound a, see (24), since the *entropy* remains constant [16]. As a consequence, across a rarefaction wave the variation in $\mathcal{M}$ is not determined by the variation in ρ, but by the variation in v.

Thus, we employ in the mentioned case the condition

$$jump\ in\ Mach\ number: \qquad \mathcal{M}_l > \mathcal{M}_m > \mathcal{M}_r, \qquad (25)$$

complementing (23). In the case $\rho_x > 0$, we test for the *entropy S* given by

$$S = c_v \ln \left(\frac{p}{\rho^\gamma} \right), \qquad (26)$$

where $c_v = constant$ is the specific heat at constant volume of a considered gas. It is well-known, see e.g. [13, 16], that entropy, and, hence p/ρ^γ, stays constant across a rarefaction wave, whereas it displays a jump at a contact wave. Thus, we complement condition (23) by testing in the indicated case, since ln is monotone for positive arguments, for a simplified version of S, i.e., $s := p/\rho^\gamma$:

$$entropy\ monotonicity: \qquad s_l > s_m > s_r. \qquad (27)$$

Within Figure 4 we observe the effect of the selective filtering of the contact discontinuity, where, in this example, the conditions (23) and (25) are in use. Obviously, the desired outcome is achieved.
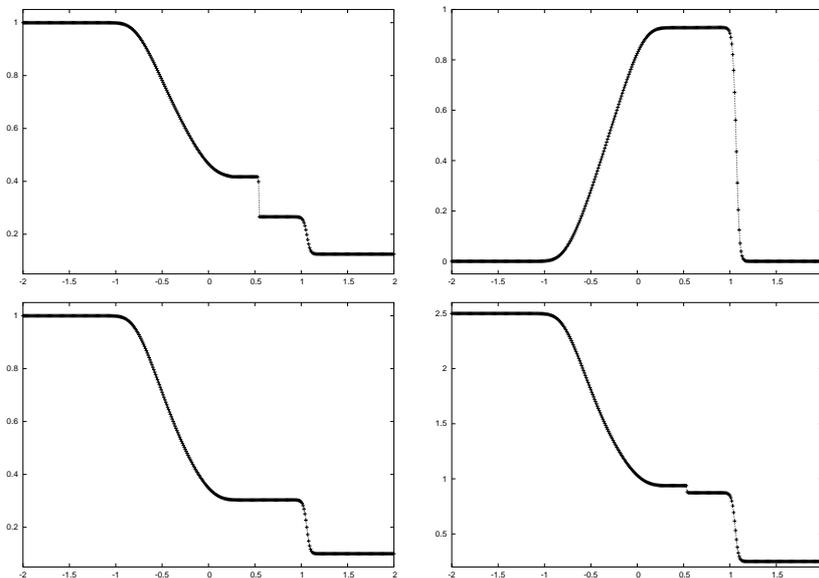

Figure 4: Selective filtering of the contact discontinuity. **Left column:** density (top) and pressure (bottom). **Right column:** velocity (top) and total energy (bottom).

11

3.4 Coupling of variables

As already stated, the indicators introduced within the last two sections are used to determine the values of the *marker variable M*, see (10)-(17). The question remains, how to apply the scalar filtering process to the usually coupled variables of a system of equations.

First of all, let us emphasize, that it is necessary to save the *unfiltered numerical solution*

$$\left\{ \left(\rho_j, \, (\rho v)_j, \, (\rho E)_j \right)^T \right\}_{j=0, \, \dots, \, N} \tag{28}$$

for use as a *reference data set* throughout the filtering procedure. This is no restriction, rather than that, it is quite natural to keep original data until a filtering procedure is completely finished.

The reason for the creation of a reference data set is explained easily by use of an example. For instance, if we would first filter in the density variable ρ and afterwards in ρv, and save the corresponding, filtered new data set as reference data for the filtering steps in the other variables, we would not filter a shock in the energy density variable ρE anymore: the velocity v obtained from the momentum ρv, see (22), does after application of the filter not indicate a filtering region of two or more contiguous cells.

Having saved the initial data for the filtering as reference data set, the variables of interest can be safely decoupled and treated by the scalar filtering process in a completely independent fashion. For instance, once having defined

$$Q_j^0 := \rho_j, \quad 0 = 1, \, \dots, \, N, \tag{29}$$

the process described via (10)-(17) can commence, yielding finally a data set

$$\left\{ \rho_j^{filtered} \right\}_{j=0, \, \dots, \, N}. \tag{30}$$

In the other variables of interest, the process can be applied, successively, in exactly the same fashion. Thus, let us stress, that the creation of the reference data set solves the coupling problem for filtering.

Let us also note, that by the complementing conditions (22) and (23), there is no problem in using shock/contact postprocessing in any combination of successively applied steps. In our algorithm, we have first filtered all shocks creating thereby a new set of reference data, followed by filtering contact discontinuities.

The result of a combined procedure is given via Figure 5 in comparison with the original numerical solution featuring diffusive artefacts. As observable, the discontinuous solution features are approximated with optimal accuracy.
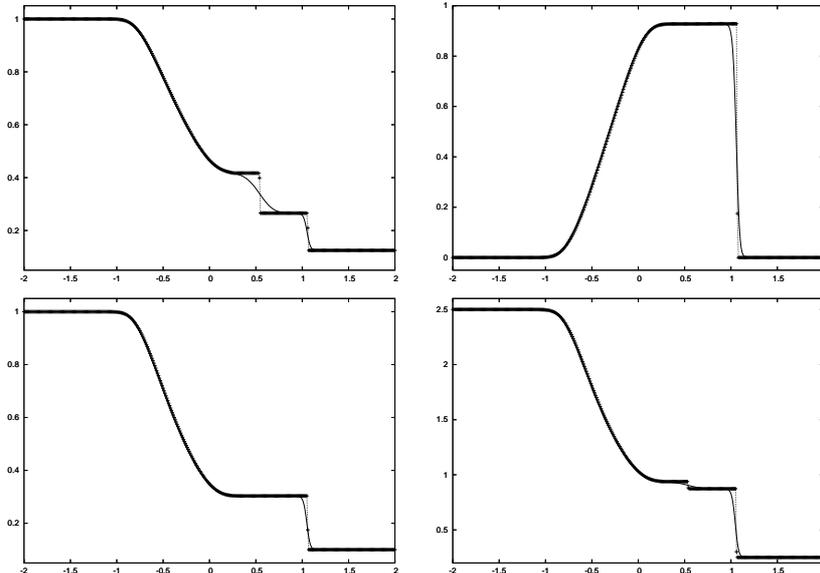
Figure 5: Filtering of all discontinuities. **Left column:** density (top) and pressure (bottom). **Right column:** velocity (top) and total energy (bottom).

4 Further numerical tests

In this section, we show the postprocessed results of two classical numerical test cases: the Woodward-Colella blast wave problem and the so-called Lax test case, see [13, 16].

4.1 The Woodward-Colella blast wave problem

The so-called blast wave problem due to Woodward and Colella is defined by use of the initial conditions

$$(\rho, \, v, \, p)^T = \left\{ \begin{array}{lll} (1, \, 0, \, 1000)^T & : & 0 < x \leq 0.1 \\ (1, \, 0, \, 0.1)^T & : & 0.1 < x < 0.9 \\ (1, \, 0, \, 100)^T & : & 0.9 \leq x < 1 \end{array} \right. , \qquad (31)$$

together with reflecting boundary conditions.

For demonstration purposes, we apply the mLF as well as the NT scheme at the problem, and we compare the corresponding non-postprocessed numerical solutions with their postprocessed counterparts. The solutions are given and compared at $t = 0.1$. In order to achieve a reasonable resolution also with the first-order scheme, which is necessary in order to achieve efficiently
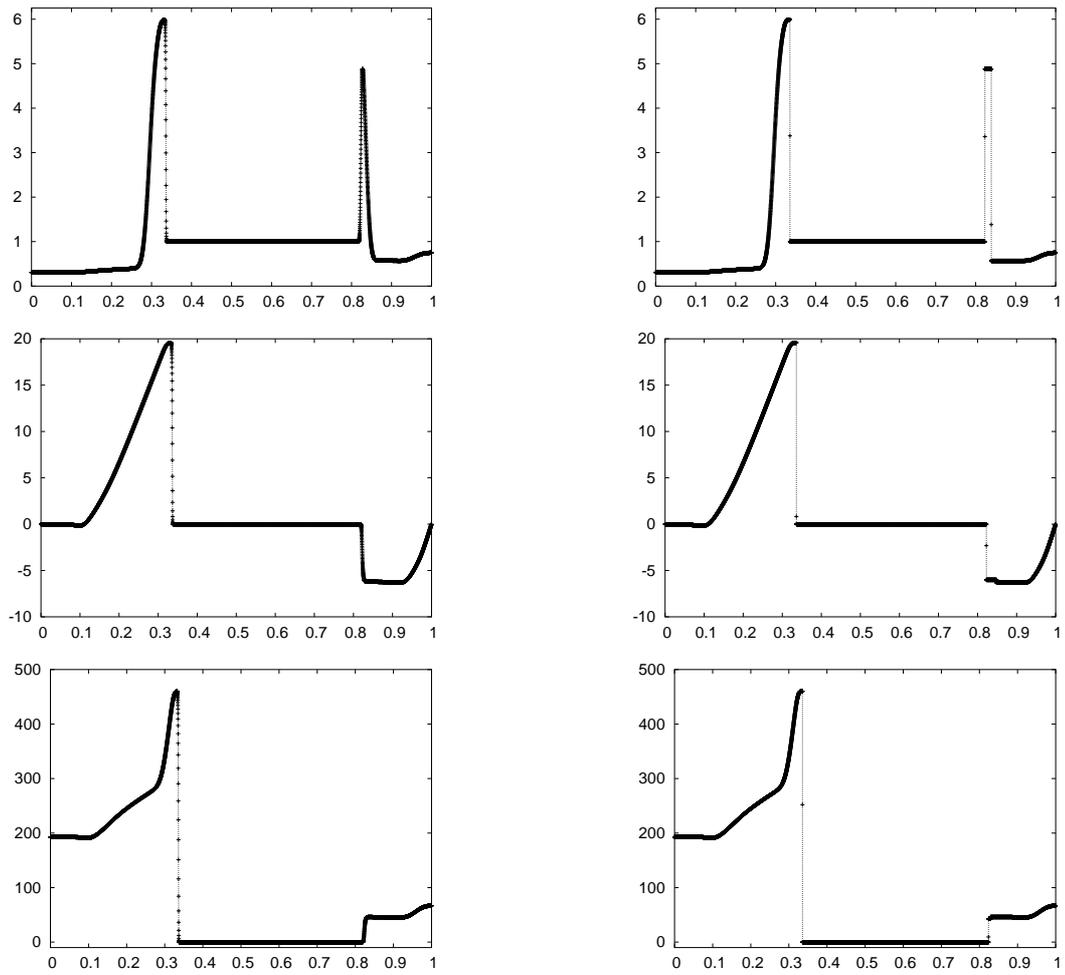
13

Figure 6: Approximation of the Woodward-Colella blast wave test case by the mLF scheme. Comparison of states (left column) before and (right column) after filtering. **Top row:** density. **Middle row:** velocity. **Bottom row:** pressure.

14

working indicator procedures, we employ $\Delta x = 0.000125$ and the usual CFL condition.

In Figure 6 we give a comparison between processed and non-processed solutions of the mLF scheme, displayed in terms of the primitive variables. The postprocessed solutions show analogous properties as in the test case used within the basic discussion.

The results displayed in Figure 7 are given analogously to those in Figure 6, using here the NT scheme from [14]. As it is observable, it is recommended in the discussed test case to use, at least, a second-order high-resolution scheme: the height of the peaks observable here, especially of the right one, is strongly influenced by the accuracy of the underlying method. Evidently, also when using the NT scheme to generate the initial data set for filtering, the postprocessing improves the solution significantly.

4.2 The Lax test case

The Lax test case, see e.g. [16], is given by use of the initial conditions

$$(\rho,\, v,\, p)^T = \left\{ \begin{array}{ll} (0.445,\, 0.698,\, 3.528)^T & : \quad 0 < x \leq 0.5 \\ (0.5,\, 0,\, 0.571)^T & : \quad 0.5 < x \leq 1 \end{array} \right. , \qquad (32)$$

together with transparent boundary conditions.

We only show results using the mLF scheme for generating initial data for filtering, since there is no observable difference to filtering results generated via use of the NT scheme. The unfiltered and filtered numerical solutions are compared at $t = 0.15$, see Figure 8, where we employed $\Delta x = 0.0005$ and a usual CFL condition within the simulation. We observe also here the desired filter effect.

5 Conclusion

By use of basic physical principles and a simple discretisation of the shock filter model developed in [4], we have successfully applied the shock filter to numerical solutions of hyperbolic systems of conservation laws.

For generating unfiltered data, we have used first- and second-order schemes. In some test cases, already a blunt application of the first-order scheme is enough to obtain reasonable filtered solutions, while in general the use of a second-order scheme is advantageous since it yields, especially, a more accurate resolution of smooth parts.

It is in general necessary to employ a discretisation accurate enough to give reliable values used for the indicator procedure; this is clear since any filter
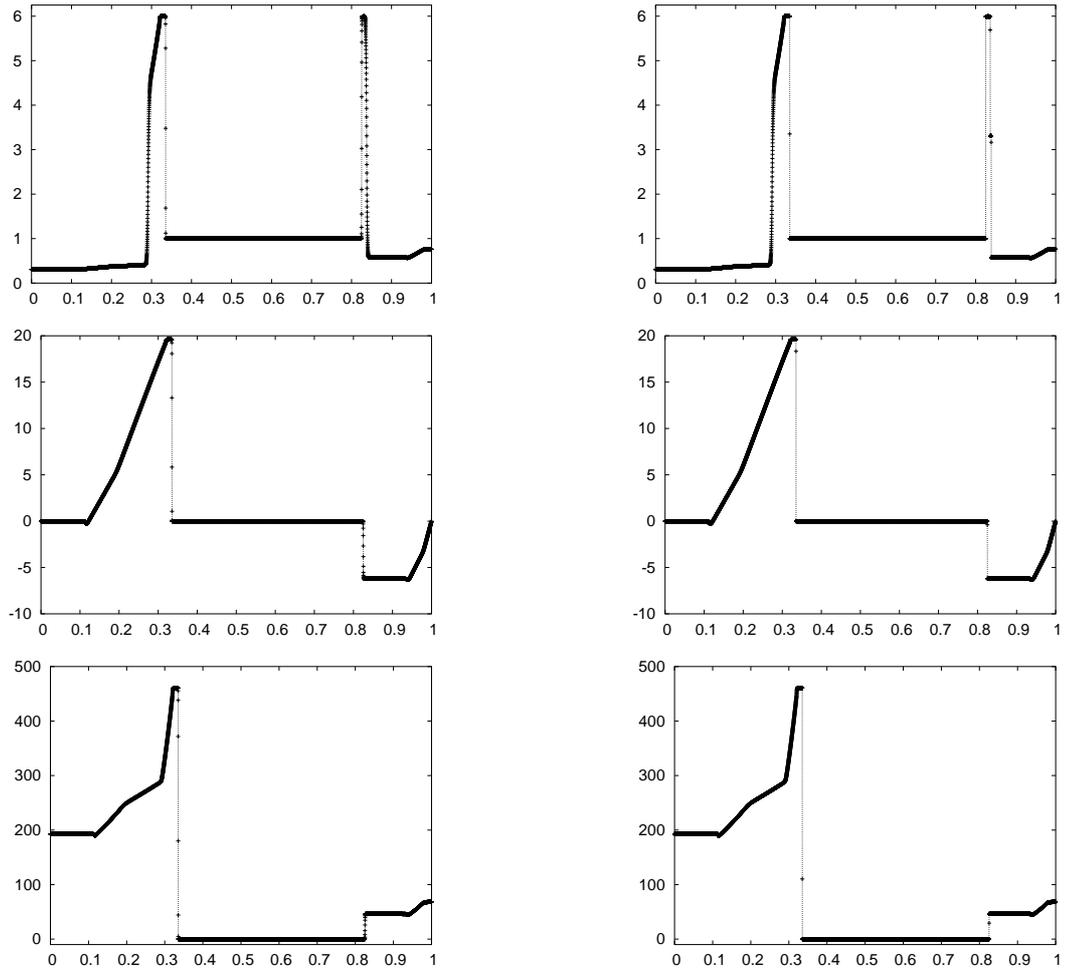
Figure 7: Approximation of the Woodward-Colella blast wave test case by the NT scheme. Comparison of states (left column) before and (right column) after filtering. **Top row:** density. **Middle row:** velocity. **Bottom row:** pressure.
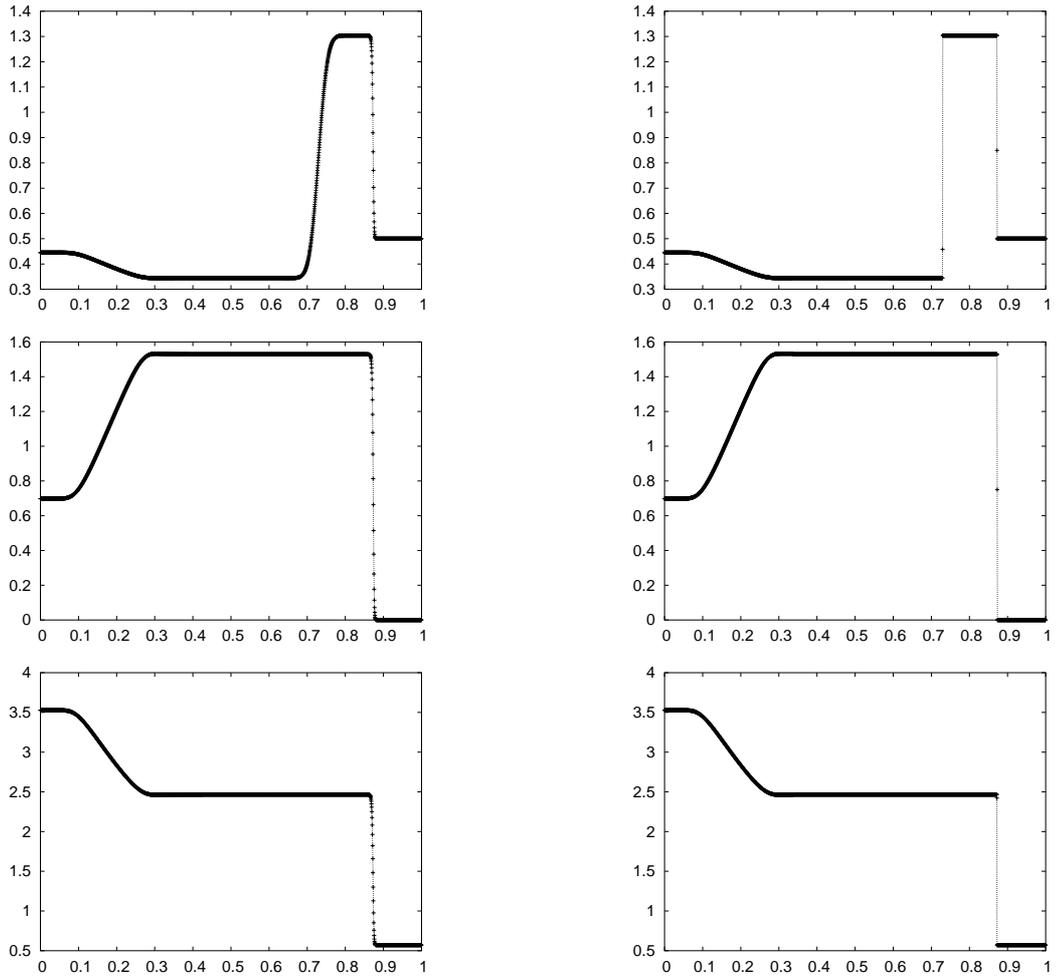
16

Figure 8: Approximation of the Lax test case by the mLF scheme. Comparison of states (left column) before and (right column) after filtering. **Top row:** density. **Middle row:** velocity. **Bottom row:** pressure.

can only filter what is actually given. Thus, in intricate test cases, the grid has to be as fine as when using any other reasonable method. However, it seems to be not incongruous, that in such cases the application of a postprocessing as presented in this work in combination with a scheme of second or medium order can be more efficient than the use of a method of very high order if the latter is only chosen in order to capture discontinuities accurately. A higher-dimensional extension of the filter is possible, however, there are several non-trivial options for the discretisation of the shock filter. The indicator we used here can be employed without a problem in higher dimensions by selecting locally proper directions for a comparison of data. This can be achieved, e.g., via methods from image processing.

6   Acknowledgements

References

[1] Boris, J.P., and Book, D.L. (1973): Flux-Corrected Transport I: SHASTA, a fluid-transport algorithm that works. *J. Comp. Phys.* **11**, pp. 38-69

[2] M. Breuß (2006): An analysis of discretisations of inverse diffusion equations. To appear in Computing Letters.

[3] M. Breuß and M. Welk (2006): Staircasing in Semidiscrete Stabilised Inverse Diffusion Algorithms. Available as Technical Report No. 165, Department of Mathematics, Saarland University. Submitted.

[4] M. Breuß and M. Welk (2006): A conservative shock filter model and its use for the numerical approximation of conservation laws. Applied Mathematics Letters **19**, pp. 954-959

[5] Engquist, B., Lotstedt, P., Sjogreen, B. (1989): Nonlinear Filters for Efficient Shock Computation. Math. Comp. **52**, pp. 509-537

[6] Gilboa, G.G., Sochen, N.A., Zeevi, Y.Y. (2002): Regularized Shock Filters and Complex Diffusion. In: A. Heyden et al. (Eds.): ECCV 2002, LNCS 2350, Springer-Verlag Berlin Heidelberg, pp. 399-413

[7] Godlewski, E., Raviart, P.-A. (1991): Hyperbolic systems of conservation laws. Ellipses

[8] Grahs, T., Meister, A., Sonar, Th. (2002): Image processing for numerical approximations of conservation laws: Nonlinear anisotropic artificial dissipation. SIAM J. Sci. Comput., **5**, pp. 1439–1455

[9] Hirsch, C. (1988): Numerical Computation of Internal and External Flows, Volume 1, Fundamentals of Numerical Discretization. Wiley-Interscience

[10] Hirsch, C. (1988): Numerical Computation of Internal and External Flows, Volume 2, Computational Methods for Inviscid and Viscous Flows. Wiley-Interscience

[11] D. Kuzmin, R. Löhner and S. Turek (Eds.): *Flux-Corrected Transport.* Springer-Verlag, 2005

[12] Lax, P. (1973): Hyperbolic Systems of Conservation Laws and the Mathematical Theory of Shock Waves. SIAM CBMS-NSF Regional Conference Series in Applied Mathematics **11**

[13] LeVeque, R.J. (2002): Finite Volume Methods for Hyperbolic Problems. Cambridge University Press

[14] Nessyahu, H., Tadmor, E. (1990): Non-oscillatory central differencing for hyperbolic conservation laws. J. Comput. Phys., **87**, pp. 408-436

[15] Osher, S., Rudin, L.I. (1990): Feature-oriented image enhancement using shock filters. SIAM J. Num. Anal., **27**, pp. 919–940

[16] Wesseling, P. (2001): Principles of Computational Fluid Dynamics. Springer Series in Computational Mathematics **29**, Springer-Verlag